Suppression Sidelobes of MIMO Radar with Distinctive Piecewise Non-linear Frequency Modulation Sub-carrier

Yujiu Zhao[a], Xingyu Lu[a], Matthew Ritchie [b], Weimin Su[a] and Hong Gu[a]

[a] Nanjing University of Science and Technology ,Department of Electronic and Optical Engineering, Nanjing 210094, Jiangsu, People's Republic of China; [b] University College London, Department of Electronic and Electrical Engineering, London, WC1E 7JE, United Kingdom.;

ABSTRACT
High sidelobes exist in normal multiple-input multiple-output (MIMO) radar waveforms, which utilize linear frequency modulation (LFM) or non-linear frequency modulation (NLFM) waveforms with the same subcarrier durations. Since the waveforms have the same expression, and each segment of the subcarriers can be only controlled by a few parameters to make them distinctive. This will cause comparatively high auto-correlation sidelobes in each zone of subcarriers. In order to suppress the sidelobes, new piecewise NLFM waveforms have been proposed in this paper. These novel MIMO radar waveforms are composed of three different kinds of subcarriers with totally different mathematical expressions. This is verified by the fact that the cross-correlation sidelobes between different subcarriers are much lower than the auto-correlation of each subcarriers. In addition, the number of MIMO radar waveforms has been improved significantly. As different subcarriers have their own controllable parameters, a genetic algorithm will be applied to generate the novel MIMO radar waveforms. Numerical results demonstrate the effectiveness that the auto-correlation sidelobes and the cross-correlation sidelobes of our proposed waveforms are reduced.

KEYWORDS
Auto-correlation, cross-correlation, multiple-input multiple-output (MIMO) radar, non-linear frequency modulation, waveform design.

1. Introduction

Multiple Input Multiple Output (MIMO) radar systems have been applied into many applications including synthetic aperture radar (SAR) imaging, target detection and target tracking problems in recent years(Cerutti-Maori et al. 2014; Hu et al. 2018; Krieger 2014; Moo et al. 2013; Tarchi et al. 2013). MIMO waveforms can improve the spatial resolution, extend image swaths, and provide novel modes to solve the problem in real radar systems. With the increasing availability of array hardware of a greater number of channels, the applicability of MIMO radars has become more and more feasible. One of the most significant challenges in MIMO radar is reducing mutual interference between different signals transmitting from different antennas is also a

---

CONTACT Hong Gu. Email: gh_student_sub@126.com

significant task. Therefore, designing diverse waveforms plays an important part in MIMO radar systems.

There are three key categories of methods to design MIMO radar waveforms, all of which have been developed in recent decades. The first category of waveform design is to take advantage of a priori information of a target, such as range and target angle to generate adaptive waveforms for cognitive radars. Minimizing mean squared error (MMSE) is one of these approaches used to design the waveforms in linear systems(Yang et al. 2007a,b), and it can also been applied into non-linear systems in Herbert et al. (2018). The second category of waveform design is focused on designing a transmitting beampattern by optimizing the waveform covariance matrix, and the transmitted waveforms are derived from the acquired covariance matrix(Fuhrmann et al. 2008; Stoica et al. 2008). The peak sidelobe level can be suppressed by maximizing the difference in the process of synthesizing the beampattern(Fan et al. 2018; Hua et al. 2013). The last category of waveform design is to base the design of orthogonal waveforms, which are generated directly in the spectral domain. Different kinds of waveforms can be applied in the subcarriers of MIMO radar signals(Song et al. 2010). Phase-coded waveforms are proposed in(Cao et al. 2015), which have extremely low range cross-correlation sidelobes (CSLs). This kind of waveform can be simulated with good performance, but it's hard to apply with real equipment. Frequency-coded waveforms include orthogonal frequency division multiplexing (OFDM) waveforms are proposed in (Kim et al. 2015; Wang et al. 2015; Wang 2015), which can produce constant modulus waveforms. However, perfect orthogonal waveforms do not exist when there are different time delays in each received signal, and they are also very sensitive to Doppler shift.

Therefore, frequency modulated waveforms without strict orthogonality are proposed in (Gao et al. 2016), they are composed of piecewise linear frequency modulation (LFM) waveformsGao et al. (2016), and piecewise non-linear frequency modulation(NLFM) waveforms are also used as the subcarriers in (Gao et al. 2017). However, all the proposed waveforms in (Gao et al. 2016, 2017) are composed of the same kind of subcarrier, and they have the same expression and can only change their durations and chirp rates using a few controllable parameters. Meanwhile, because there are pulse intervals between each subcarrier, the full time duration is not utilized. In order to get rid of the gap between each subcarrier, modifications to Gao's piecewise non-linear frequency modulation (PNLFM) MIMO radar signals have been proposed improved, which have no gap between each subcarrier. However, it will produce some repetitive high sidelobes, and limit the diversity of waveforms.

In order to solve this problem, we propose a novel piecewise non-linear frequency modulation (PNLFM) waveform. It is known that NLFM waveforms have lower APSLs and CSLs than LFM waveforms Boukeffa et al. (2011). In addition, the CSLs between different kinds of waveforms can be achieved lower. In this paper, we propose MIMO radar waveforms which are composed of three different kinds of PNLFM subcarriers and each subcarrier has its own controllable parameters. Except for the novel PNLFM waveform proposed here, two other piecewise waveforms proposed in (Gao et al. 2017; Zhao et al. 2018) have been applied to our MIMO radar signals. Since there are so many controllable parameters in the optimization function, a genetic algorithm is utilized to optimize the sidelobes of our proposed waveforms. Numerical simulations can demonstrate that the repetitive high sidelobes have been removed with distinctive subcarriers in a single MIMO radar signal, improving the orthogonality, and therefore the number of MIMO radar signals is possible to use jointly. In Section 2, we introduce two kinds of PNLFM waveforms, and propose our new PNLFM waveforms. In Section

3, our MIMO radar system model and MIMO radar ambiguity function are introduced. In Section 4, a genetic algorithm is applied to optimize our fitness function, and generate our proposed MIMO radar signals. In Section 5, numerical simulations results are shown to verify that our proposed MIMO radar signals achieve better performance. In Section 6, it is the conclusion.

2. Piecewise NLFM waveform design

In this section, we first review two kinds of PNLFM waveforms proposed in (Gao et al. 2017; Zhao et al. 2018). Next, we introduce the design method of our new PNLFM waveforms.


2.1. *Introduction of some PNLFM waveforms*

The time-frequency scheme of PNLFM waveforms are shown in Figure (1). It can be seen that all the piecewise waveforms have a similar form, and the only difference is that the second segments of each piecewise waveform have different expressions. In order to combine these waveforms into a single MIMO radar waveform, a more common expression has been proposed. Distinctive waveforms can be expressed in Equation (1). Figure 1(a) shows the PNLFM waveform proposed in (Gao et al. 2017), which are labelled as Gao's PNLFM waveforms $S_{G(m,l)}(t)$, where m is the number of MIMO radar waveforms, l is the number of subcarriers, and t is the time parameter of MIMO radar waveforms. Figure 1(b) shows the PNLFM waveform proposed in (Zhao et al. 2018), which are labelled as Zhao's PNLFM waveforms $S_{Z(m,l)}(t)$. Figure 1(c) shows the PNLFM waveform proposed in this paper, which are the newly proposed PNLFM waveforms $S_{O(m,l)}(t)$. The common expression can be shown as follows:

$$S_{C(m,l)}(t) =$$
$$\begin{cases} \mathrm{e}^{j2\pi t f_{1,m,l}} \mathrm{e}^{j\pi\mu_{m,l}t^2}, & -\dfrac{T_\mathrm{p}}{2} \leq t < -\dfrac{T_\mathrm{p}}{2} + \Delta_{m,l}, \\[2mm] \mathrm{e}^{j2\pi t f_c} \mathrm{e}^{j\varphi_{m,l}(t)}, & -\dfrac{T_{m,l}}{2} \leq t \leq \dfrac{T_{m,l}}{2}, \\[2mm] \mathrm{e}^{j2\pi t f_{3,m,l}} \mathrm{e}^{j\pi\mu_{m,l}t^2}, & \dfrac{T_\mathrm{p}}{2} - \Delta_{m,l} < t \leq \dfrac{T_\mathrm{p}}{2}. \end{cases} \quad (1)$$

where T_p is defined as the duration of each distinctive subcarrier, B_p is defined as the bandwidth of each distinctive subcarrier, it is important to note that all the distinctive subcarriers have the same duration and bandwidth. Since each new MIMO radar waveform is composed of a sequence of distinctive waveforms, the total number in our new MIMO radar waveforms can be defined as M and $0 \leq m \leq M - 1$. The total sequence number in each new MIMO radar waveform can be defined as L and $0 \leq l \leq L - 1$. Assuming that each distinctive waveform has the same expression in the first and third segment, therefore, the subcarrier bandwidth of the first and third segment is defined as $\Omega_{m,l} = \delta_{m,l}B_\mathrm{p}/2$ and $0 < \delta_{m,l} < 2$.

Here a little improvement has been made on the duration of the second segment $T_{m,l}$ in each distinctive subcarrier of Gao's PNFLM waveform. In the original expression, the duration of the second segment equals the subcarrier duration multiplies a fixed fractional number, while in this paper the fractional number is random within a certain range, and it can increase the degrees of freedom and improve the performance. Thus,

3
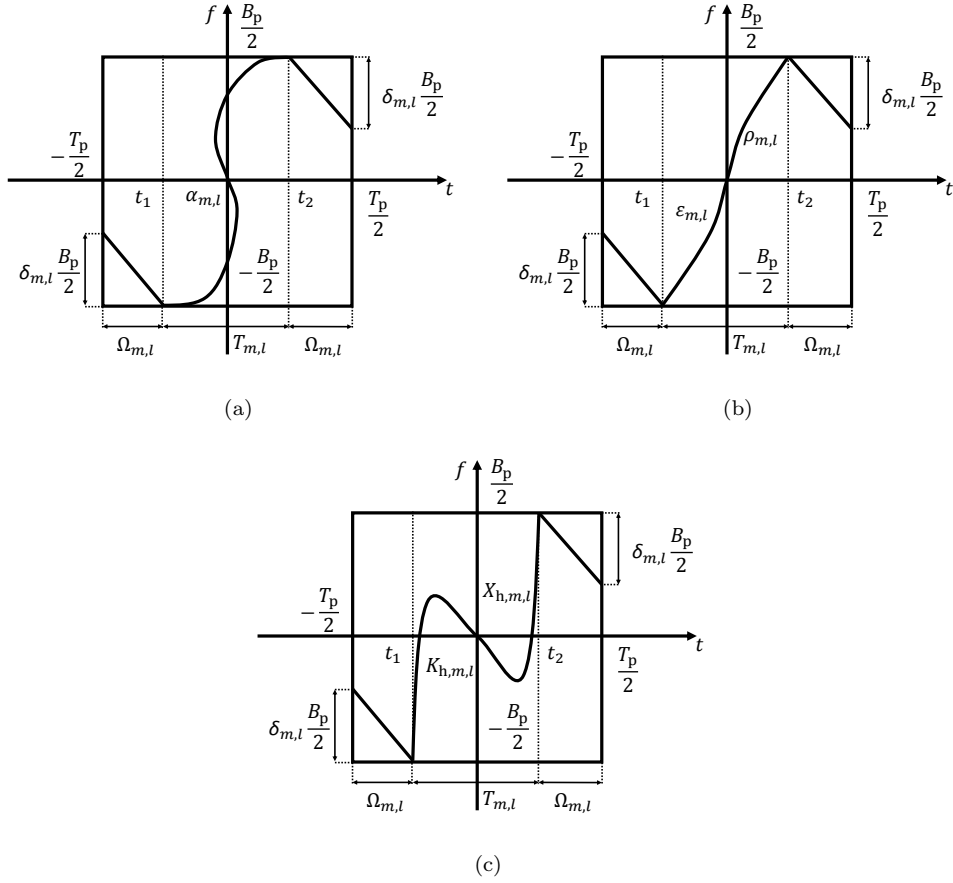
Figure 1. Time-frequency scheme of PNLFM waveform (a) Gao's PNLFM waveform. (b) Zhao's PNLFM waveform. (c) Our proposed PNLFM waveform.

4

the common expression of the duration in the second segment of each distinctive waveform can be defined as $T_{m,l} = \eta_{m,l}T_{\mathrm{p}}$ and $0 < \eta_{m,l} < 1$. The duration of the first and third segment in each distinctive subcarrier can be expressed as $\Delta_{m,l} = (T_{\mathrm{p}} - T_{m,l})/2$. In addition, The chirp rates of the first and third segment are the same and can be expressed as $\mu_{m,l} = -\xi_{m,l}\Omega_{m,l}/\Delta_{m,l}$, where $\xi_{m,l}$ is the parameter to control the polarity of chirp rate, when l is odd, the polarity of chirp rate in the second segment of the subcarrier is positive and $\xi_{m,l} = 1$, otherwise when l is even and $\xi_{m,l} = -1$. The subcarrier frequency of each segment can be shown as follows:

$$
\begin{aligned}
f_{d,m,l} =& f_c + (d-2)\xi_{m,l}\left(\frac{\Omega_{m,l}T_{\mathrm{p}}}{2\Delta_{m,l}} + \frac{B_{\mathrm{p}}}{2} - \Omega_{m,l}\right) \\
d =& 1,3
\end{aligned}
\tag{2}
$$

According to the analysis mentioned above, when it comes to Gao's PNLFM waveforms which is shown in Figure 1(a), the phase of the second segment can be expressed as:

$$
\varphi_{m,l}(t) = \varphi_{G(m,l)}(t) = \frac{2\pi\xi_{m,l}w_{m,l}}{g_{m,l}h_{m,l}}\sec(g_{m,l}t)
\tag{3}
$$

where $w_{m,l} = \alpha_{m,l}B/\pi$, $g_{m,l} = 2\arctan\left(\pi/2\alpha_{m,l}\right)/T_{m,l}$, and $h_{m,l} = \sec\left(g_{m,l}T_{m,l}/2\right)$. For Zhao's PNLFM waveforms which are shown in Figure 1(b), the phase of the second segment can be expressed as:

$$
\begin{aligned}
\varphi_{m,l}(t) =& \varphi_{Z(m,l)}(t) = \\
&\frac{\pi\xi_{m,l}\rho_{m,l}B_{\mathrm{p}}}{\zeta}\ln\left(\mathrm{e}^{\frac{1}{2\rho_{m,l}}} + \epsilon_{m,l}\cosh\left(\frac{\zeta t}{\rho_{m,l}}\right) - \epsilon_{m,l}\mathrm{e}^{\frac{1}{2\rho_{m,l}}}\right)
\end{aligned}
\tag{4}
$$

where $\zeta = 20/T_p$, the duration and the chirp rate of second segment in Zhao's PNLFM waveform can be controlled by $\rho_{m,l}$ and $\epsilon_{m,l}$, respectively.

2.2. *Designing a novel piecewise NLFM waveform*

Following the analysis above, we focus on designing the second segment in the novel PNLFM waveforms. A novel NLFM waveform is proposed here, the expression for the time-frequency scheme is given as:

$$
\frac{\mathrm{d}f(t)}{\mathrm{d}t} = \mu(t) = \mu_{\mathrm{h}} - \frac{\mu_{\mathrm{h}} - \mu_{\mathrm{l}}}{\left[\left(t - \frac{T_{\mathrm{se}}}{2}\right)/\left(T_{\mathrm{h}} - \frac{T_{\mathrm{se}}}{2}\right)\right]^{2n}}, t \in [0, T_{\mathrm{se}}]
\tag{5}
$$

where $f(t)$ is the frequency function of the second segment in our proposed PNLFM waveforms, and $\mu(t)$ is the time-frequency function. μ_{h} is the upper bound of $\mu(t)$, μ_{l} is the chirp rate in the pulse center, T_{se} is the duration of the novel NLFM waveform, $T_{\mathrm{h}} \in [0, T_{\mathrm{se}}/2)$, and n is a positive integer. In order to simplify the expression, we define $x = t/T_{\mathrm{se}}$, $\tilde{\mu} = B_{\mathrm{p}}/T_{\mathrm{se}}$, $X_{\mathrm{h}} = T_{\mathrm{h}}/T_{\mathrm{se}}$, $K_{\mathrm{h}} = \mu_{\mathrm{h}}/\tilde{\mu}$, and $K_{\mathrm{l}} = \mu_{\mathrm{l}}/\tilde{\mu}$, then the expression can be shown as:

$$
k(x) = \frac{\mu(xT_{\mathrm{se}})}{\tilde{\mu}} = K_{\mathrm{h}} - (K_{\mathrm{h}} - K_{\mathrm{l}})Y_{n,X_{\mathrm{h}}}(x)
\tag{6}
$$

5

$$Y_{n,X_h}(x) = \frac{1}{1 + \left(\frac{2x-1}{2X_h-1}\right)^{2n}} \tag{7}$$

where $x \in [0,1]$, and T_{se} has been eliminated. Assuming that the normalized starting frequency is $f(0) = 0$, and the normalized ending frequency is also a fixed value, $v(1) = 1$, the instantaneous frequency can be expressed as:

$$f(xT_{se}) = f(0) + \int_0^{xT_{se}} \mu(z)\mathrm{d}z = B_p \int_0^x k(\tau)\mathrm{d}\tau \tag{8}$$

$$v(x) = \int_0^x [K_h - (K_h - K_l)Y_{n,X_h}(\tau)]\mathrm{d}\tau \tag{9}$$

where $z = \tau T_{se}$. Assuming that $Z_{n,X_h}(x) = \int_0^x Y_{n,X_h}(\tau)\,\mathrm{d}\tau$, then

$$v(1) = K_h - (K_h - K_l)Z_{n,X_h}(1) \tag{10}$$

it can be known that if we obtain the value of K_h then K_l is also known, and vice versa. Furthermore, we can get that:

$$v(x) = K_h x - (K_h - 1)\frac{Z_{n,X_h}(x)}{Z_{n,X_h}(1)} \tag{11}$$

Therefore, the instantaneous phase of our new proposed NLFM waveforms can be expressed as:

$$\begin{aligned}\varphi(xT_{se}) &= 2\pi \int_0^{xT_{se}} f(z)\mathrm{d}z = 2\pi B_p T_{se} \int_0^x v(\tau)\mathrm{d}\tau \\ &= 2\pi B_p T_{se}\left[\frac{K_h x^2}{2} - \frac{K_h-1}{2}\int_0^x \frac{Z_{n,X_h}(\tau)}{Z_{n,X_h}(1)}\mathrm{d}\tau\right]\end{aligned} \tag{12}$$

There are three controllable parameters n, X_h and K_h. In Equation (12), there is a double integration expression, which is computationally complex. In order to further simplify this function, the power exponent $n = 2$ is fixed. In Equation (7), it is assumed that $w = \frac{2x-1}{2X_h-1}$, hence $Z_{n,X_h}(x)$ can be transformed into that:

$$\begin{aligned}\int Y_{2,X_h}(\tau)\mathrm{d}\tau = \quad Q(x) &= \frac{2X_h-1}{8\sqrt{2}}\left[-2\arctan\left(1-\sqrt{2}w\right)\right.\\ &\quad +2\arctan\left(1+\sqrt{2}w\right) - \ln\left(1 - \sqrt{2}w + w^2\right) \\ &\quad \left.+ \ln\left(1 - \sqrt{2}w + w^2\right)\right]\end{aligned} \tag{13}$$

$$Z_{2,X_h}(x) = \int_0^x Y_{2,X_h}(\tau)\mathrm{d}\tau = Q(x) - Q(0) \tag{14}$$

According to the analysis above, and the double integration function in Equation (12), this can be further simplified into:
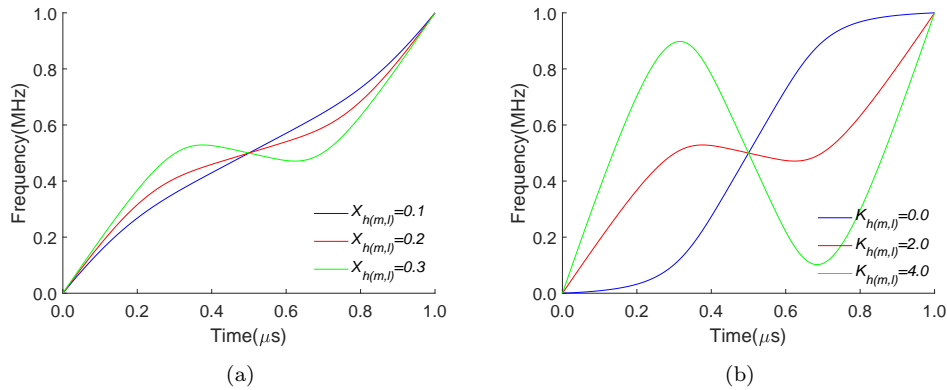
$$
\begin{aligned}
\int Z_{2,X_\mathrm{h}}(\tau)\mathrm{d}\tau &= \int Q(\tau) - Q(0)\mathrm{d}\tau = P(x) \\
&= \left(\tfrac{2X_\mathrm{h}-1}{2}\right)^2 \times \tfrac{1}{4\sqrt{2}}\left\{2\left(\sqrt{2}-w\right)\times\arctan\left(1-\sqrt{2}w\right)\right. \\
&+2\left(\sqrt{2}+w\right)\times\arctan\left(1+\sqrt{2}w\right) \\
&+w\left[-\ln\left(1-\sqrt{2}w+w^2\right)+\ln\left(1+\sqrt{2}w+w^2\right)\right]\big\} \\
&-Q(0)\,w\tfrac{2X_\mathrm{h}-1}{2}
\end{aligned}
\tag{15}
$$

$$
\int_0^x Z_{2,X_\mathrm{h}}(\tau)\mathrm{d}\tau = P(x) - P(0)
\tag{16}
$$

Finally, the function of our novel NLFM waveform in the second segment of PNLFM waveforms in (12) can be expressed as:

$$
\begin{aligned}
\varphi_{m,l}(t) &= \varphi_{O(m,l)}(t) = \varphi_{m,l}(xT_\mathrm{se}) \\
&= 2\pi B_\mathrm{p}T_\mathrm{se}\left[\tfrac{K_{h(m,l)}x^2}{2} - \left(K_{h(m,l)}-1\right)\tfrac{P(x)-P(0)}{Q(x)-Q(0)}\right]
\end{aligned}
\tag{17}
$$

where the T_se represents the duration of the second segment of the subcarrier in

Figure 2. Time-frequency scheme of the second segment in our proposed PNLFM waveform (a) $K_{h(m,l)} = 2.0$, $X_{h(m,l)} = 0.1, 0.2, 0.3$. (b) $X_{h(m,l)} = 0.3$, $K_{h(m,l)} = 0, 2, 4$.

our proposed PNLFM waveforms. The function shown in Equation (17) has two controllable parameters to change the time-frequency scheme shape of NLFM waveform, it can be regarded as the second segment of our proposed PNLFM subcarrier, and in the (m,l)th subcarriers, we define $K_{h(m,l)} = K_\mathrm{h}$ and $X_{h(m,l)} = X_\mathrm{h}$, respectively. When $K_{h(m,l)} = 2.0$, and $X_{h(m,l)} = 0.1, 0.2, 0.3$, the time-frequency scheme of the second segment in PNLFM waveform is shown in Figure 2(a). When $X_{h(m,l)} = 0.3$, and $K_{h(m,l)} = 0.0, 2.0, 4.0$, the time-frequency scheme of the second segment in PNLFM waveform is shown in Figure 2(b). The auto-correlation function (ACF) and cross-correlation function (CCF) between the introduced PNLFM waveforms mentioned above are shown in Figure 3 and all the different controllable parameters are shown in Table 1. In Figure 3(a) all the PNFLM waveforms have the same up-chirp rates $\xi_{m,l} = 1$ in the CCF, it can be observed that the CPLs in the CCF is lower than the

APSLs in the region where the time delay is near 0μs. In Figure 3(b) all the PNFLM waveforms have the down-chirp rate $\xi_{m,l} = -1$ in the CCF, and the CPLs in the CCF is also lower than the APSLs in the region where the time delay is near 0μs. Since the high repetitive sidelobes are generated by the same kind of PNLFM subcarrier in one MIMO radar signal, the distinctive subcarriers are applied to replace the same subcarrier in our new proposed MIMO radar signals and reduce the sidelobes.

Table 1. The parameters of distinctive PNLFM waveforms

$S_{O(m,l)}(t)$	$X_{h(m,l)}$	$K_{h(m,l)}$	$\delta_{m,l}$	$\eta_{m,l}$
Value	0.3	2	0.2	0.8
$S_{G(m,l)}(t)$	$\alpha_{m,l}$	$\delta_{m,l}$	$\eta_{m,l}$	
Value	2.95	0.51	0.375	
$S_{Z(m,l)}(t)$	$\rho_{m,l}$	$\epsilon_{m,l}$	$\delta_{m,l}$	
Value	0.71	0.57	0.31	

(a)

(b)
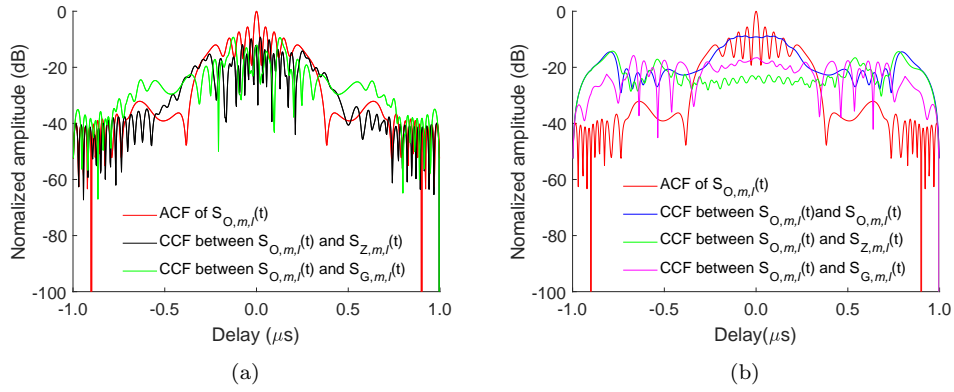
Figure 3. The ACF and CCF between different kinds of PNLFM waveforms($T_\mathrm{p} = 1\mu$s, $B_\mathrm{p} = 50$Mhz) (a) All the PNFLM waveforms have the same up-chirp rates in the CCF. (b) All the PNFLM waveforms have the opposite chirp rates in the CCF.

3. MIMO Radar Signal Model and Ambiguity Function

In this section, the time-frequency scheme of our proposed PNLFM MIMO signal is introduced. As shown in Figure 4(a), it has the same time-frequency scheme of original Gao's PNLFM MIMO radar signals, and T_r is the subcarrier repetition interval, T_p is the time duration of each subcarrier; in this case there are duration gaps between each subcarrier. As shown in Figure 4(b), the duration gaps have been eliminated, and there are three different kinds of fillings in our proposed MIMO radar signals, the orange grid represents Gao's PNLFM waveform which has been improved, the yellow grid represents Zhao's PNLFM waveform, and the green grid represents our proposed PNLFM waveform. According to the analysis in Section 2, each grid can be filled with these three kinds of PNLFM waveforms randomly, it means that our scheme can improve the diversity of MIMO radar signal significantly. In addition, each grid has the same subcarrier duration T_p and same subcarrier bandwidth B_p, respectively. There are M kinds of different non-orthogonal signals in our MIMO radar model, and each non-orthogonal signal is composed of L different subpulse PNLFM waveforms. Comparing with the waveforms proposed in (Gao et al. 2017), the number of MIMO

8

radar signal is 3^L larger than the original set. In order to simplify the processing of waveform design, assuming that $M = 4$ and $L = 8$, the subcarrier sequence number is defined as $\mathbf{Y} = \{Y_{1,1}, Y_{1,2}, \ldots, Y_{m,l}, \ldots, Y_{M,L}\}$, and they are selected randomly. When $Y_{m,l}$ is 1, $S_{C(m,l)}(t) = S_{G(m,l)}(t)$; when $Y_{m,l}$ is 2, $S_{C(m,l)}(t) = S_{Z(m,l)}(t)$; and when $Y_{m,l}$ is 3, $S_{C(m,l)}(t) = S_{O(m,l)}(t)$. The expression of our proposed radar signal can be shown as:

$$S_m(t) = \sum_{l=0}^{L-1} u(t - lT_{\mathrm{p}}) \times S_{C(m,l)}(t - lT_{\mathrm{p}}) \tag{18}$$

where $u(t)$ is an unit rectangle window function, $0 \leq l \leq L-1$, and T_{p} is the subcarrier
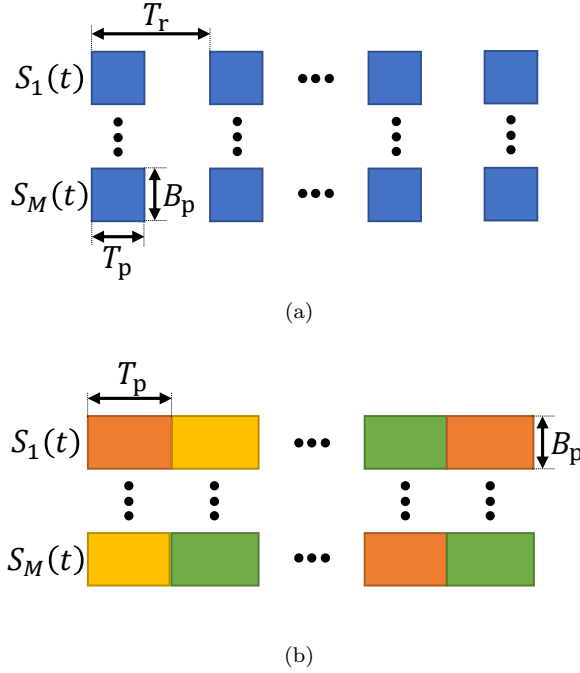
Figure 4. Time-frequency scheme of MIMO radar signal. (a) The blue grid represents original Gao's PNLFM waveform .(b) The orange grid represents Gao's PNLFM waveform which has been improved, the yellow grid represents Zhao's PNLFM waveform, and the green grid represents our proposed PNLFM waveform

duration. In addition, the subchirp rate polarities of our proposed radar signal are $\{+, -, +, -, +, -, +, -\}$. As a part of this analysis, assuming that the MIMO radar system is a collocated MIMO radar array using our proposed signals. Four transmitting and receiving antennas are used in the colocated MIMO radar array and the number of proposed radar signals is equal to the numbers of transmitting antennas. Therefore, $M = N = 4$ are the numbers of transmitting and receiving antennas, respectively. The steering vectors of the transmitting and receiving antennas are defined as follow:

$$\begin{aligned} \mathbf{V}_t(\theta) = \quad &\{1, \exp(-j\varphi_{\mathrm{t}}(\theta)), \exp(-j2\varphi_{\mathrm{t}}(\theta)), \ldots, \\ &\exp(-j(M-1)\varphi_{\mathrm{t}}(\theta))\}^{\mathrm{T}} \end{aligned} \tag{19}$$

$$\mathbf{V}_r(\theta) = \begin{aligned} &\{1, \exp(-j\varphi_\mathrm{r}(\theta)), \exp(-j2\varphi_\mathrm{r}(\theta)), \ldots, \\ &\exp(-j(N-1)\varphi_\mathrm{r}(\theta))\}^\mathrm{T} \end{aligned} \qquad (20)$$

where $\varphi_\mathrm{t}(\theta) = 2\pi d_\mathrm{t}\sin(\theta)/\lambda$, $\varphi_\mathrm{r}(\theta) = 2\pi d_\mathrm{r}\sin(\theta)/\lambda$, d_t is the distance between each transmitting antenna, d_r is the distance between each receiving antenna, θ represents the angle to the target and λ is the wavelength. The received signal at the received antenna can be expressed as $\mathbf{H}(t) = \mathbf{V}_r(\theta)\mathbf{V}_t(\theta)^\mathrm{T}\mathbf{S}(t-\tau)\exp(2\pi f_\mathrm{d}t)$, where $\mathbf{H}(t) = \{H_0(t), H_1(t), \ldots, H_{N-1}(t)\}^\mathrm{T}$, $\mathbf{S}(t-\tau) = \{S_0(t-\tau), S_1(t-\tau), \ldots, S_{M-1}(t-\tau)\}^\mathrm{T}$, τ is the time delay and f_d is the Doppler frequency. Therefore, the expression of our proposed echo signal in the nth receiving antenna can be shown as:

$$H_n(t)|_{\tau,f_\mathrm{d},\varphi(\theta)} = \sum_{m=0}^{m=M-1} \eta S_m(t-\tau)\exp(j2\pi f_\mathrm{d}t) \\ \times\exp(j2\pi\varphi(\theta)(\beta m + n)) \qquad (21)$$

where η is the target reflection coefficient, $\beta = d_\mathrm{t}/d_\mathrm{r}$ and $\varphi(\theta) = d_\mathrm{r}\sin(\theta)/\lambda$ is the normalized spatial frequency of the target. In order to achieve the target location and velocity, some corresponding matched filters are designed to get echo signal. According to the equation in Equation (21), there are three dimensions in the echo signal, which include range, Doppler, and angle.

The MIMO radar ambiguity function (AF) is an important technique to evaluate the sidelobes and resolution properties in the ACF and CCF, and it can be defined as(Chen et al. 2008):

$$\chi(\tau, f_\mathrm{d}, \varphi(\theta), \varphi'(\theta)) = \\ \left| \sum_{m=0}^{M-1} \sum_{m'=0}^{M-1} \chi_{m,m'}(\tau, f_\mathrm{d})\exp(j2\pi(\varphi'(\theta)m - \varphi'(\theta)m')\beta) \right| \qquad (22)$$

where

$$\chi_{m,m'}(\tau, f_\mathrm{d}) = \int_{-\infty}^{+\infty} S_m(t)S_{m'}^*(t-\tau)\exp(j2\pi f_\mathrm{d}t)\,\mathrm{d}t \qquad (23)$$

$$R_{S_m(t),S_{m'}(t)}(\tau) = \int_{-\infty}^{+\infty} S_m(t)S_{m'}^*(t-\tau)\,\mathrm{d}t \qquad (24)$$

$\chi_{m,m'}(\tau, f_\mathrm{d})$ is called the cross ambiguity function (CAF), and if $m = m'$, Equation (23) turns to be the AF of the mth transmitting signal. What's more, if $f_d = 0$ and $m = m'$, Equation (23) turns to be (24), and it can be called as the ACF, while if $m \neq m'$, Equation (24) can be regarded as the CCF.

## 4. Parameter Optimization in MIMO Radar with Distinctive PNLFM Waveforms

In this section, the optimization model of our new MIMO radar signal will be proposed. According to the analysis above, there are several controllable parameters in each distinctive PNLFM subcarrier. The parameter vector sets include $\mathbf{A} = \{\alpha_{1,1}, \ldots, \alpha_{m,l}, \ldots, \alpha_{M,L}\}$, $\mathbf{P} = \{\rho_{1,1}, \ldots, \rho_{m,l}, \ldots, \rho_{M,L}\}$, $\mathbf{E} = \{\epsilon_{1,1}, \ldots, \epsilon_{m,l}, \ldots, \epsilon_{M,L}\}$, $\mathbf{X}_h = \{X_{\mathrm{h},1,1}, \ldots, X_{h(m,l)}, \ldots, X_{h(m,l)}\}$,

$\mathbf{K}_h = \{K_{\mathrm{h},1,1}, \ldots, K_{h(m,l)}, \ldots, K_{h(m,l)}\}$, $\mathbf{B} = \{\delta_{1,1}, \ldots, \delta_{m,l}, \ldots, \delta_{M,L}\}$, $\mathbf{H} = \{\eta_{1,1}, \ldots, \eta_{m,l}, \ldots, \eta_{M,L}\}$, $\mathbf{Y} = \{Y_{1,1}, \ldots, Y_{m,l}, \ldots, Y_{M,L}\}$, and all of them can be used to control the shape and duration in each segment of PNLFM waveforms. In addition, the APSLs and CSLs can be suppressed by using the genetic algorithm to optimize the fitness function. The fitness function can be expressed with the parameter vectors mentioned above:

$$
\begin{aligned}
&\min_{\mathbf{A},\mathbf{P},\mathbf{E},\mathbf{X}_h,\mathbf{K}_h,\mathbf{B},\mathbf{H},\mathbf{Y}} \\
&\left\{ \sum_{m=0,\tau\neq0}^{M-1} \max \left| R_{S_m(t),S_m(t)}(\tau) \right| \right. \\
&+ \sigma_1 \sum_{m=0}^{m=M-1} \left[\sum_{\tau\neq0} \left| R_{S_m(t),S_m(t)}(\tau) \right|^2 \bigg/ \sum_{|\tau|=0.2T_p} \left| R_{S_m(t),S_m(t)}(\tau) \right|^2 \right] \\
&+ \sigma_2 \sum_{m=0}^{m=M-1} \sum_{m'=0,m'\neq m}^{M-1} \max \left| \chi_{m,m'}(\tau,f_\mathrm{d}) \right| \\
&\left. + \sigma_3 \sum_{f_\mathrm{d},\tau\neq0} \max \left| \chi(\tau,0,\varphi(\theta),\varphi'(\theta)) \right| \right\} \\
&s.t. \quad 0 < \alpha_{m,l} < 3 \quad\quad 0 < \rho_{m,l} < 1 \quad\quad 0 < \epsilon_{m,l} < 1 \\
&\quad\quad\quad 0 < X_{h(m,l)} < 0.3 \quad 0 < K_{h(m,l)} < 4 \quad 0 < \delta_{m,l} < 2 \\
&\quad\quad\quad 0 < \eta_{m,l} < 1 \quad\quad Y_{m,l} \in \{1,2,3\}
\end{aligned}
\tag{25}
$$

where σ_1, σ_2, and σ_3 are the weighted coefficients, they can be used to provide a trade-off implementation to satisfy the requirement of signals in different situations. According to the sequence number, the restriction condition of different parameters can be used to generate distinctive PNLFM waveforms. Unlike the previous expression proposed in (Gao et al. 2017), more controllable parameters are added into the fitness function, and each controllable parameter has its own restricted range. This increase the degrees of freedom in this fitness function. Equation (25) consist of four components, the first term in this expression can be described as the ACF, and it can be used to detect the target and distinguish the small target with the sidelobes. These range sidelobes and resolution can be observed by APSLs. The second term can be described as the integrated sidelobe ratio (ISLR), and it can be used to determine the energy of the main lobe in the transmitting signal. The third term represents the CCF, since our proposed MIMO radar signals are non-orthogonal in time-frequency domain, the lower cross-correlation sidleobes between different signals can be regarded as orthogonal ones approximately. The last term is the range-angle function, and the angle resolution, angle sidelobes (ASLs), the APSLs from the same angle and CSLs from different angle can be investigated.

In order to suppress the sidelobes of MIMO radar signals and optimize the fitness function, the genetic algorithm is applied to solve this problem (Liu et al. 2007). The population number, crossover rate, mutation rate and iteration number will be initialized first. A loop process from selection, mutation and evaluation will be continued until it reaches the limit of iteration number or the restriction condition of the fitness function. Then the optimized controllable parameters are obtained after the operation mention above, and the optimization model of our proposed PNLFM MIMO radar signals is output.
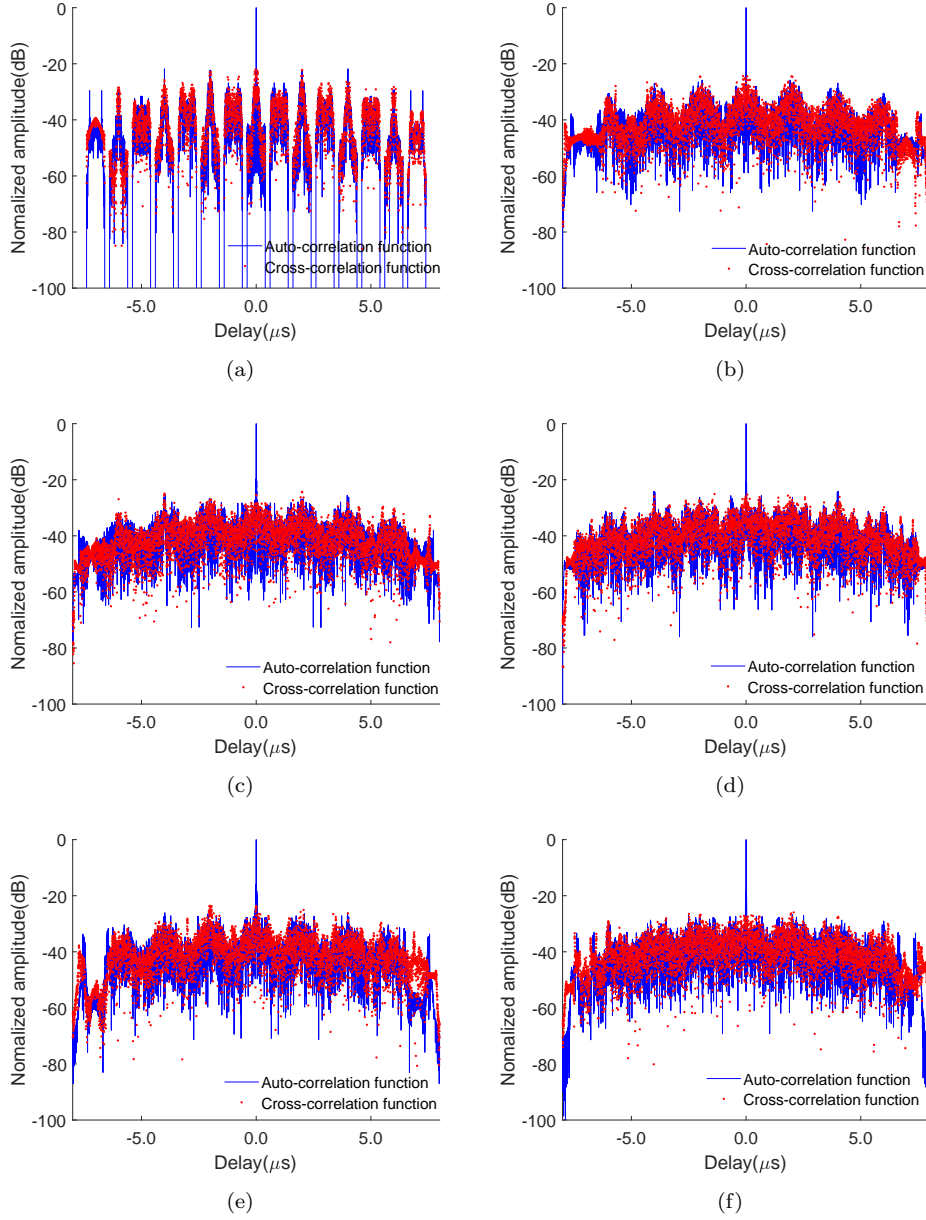
Figure 5. The ACF and CCF of PNLFM MIMO radar signals. (a) Original Gao's PNLFM MIMO radar signal. (b) Gao's PNLFM MIMO radar signal. (c) Gao's PNLFM MIMO radar signal with improvement. (d) Zhao's PNLFM MIMO radar signal. (e) New PNLFM MIMO radar signal. (f) PNLFM MIMO radar signal with distinctive waveforms.

5. Simulation and analysis

In this section, numerical simulation results of our proposed PNLFM MIMO radar signals are shown to illustrate the effectiveness of our method, and these are compared with original Gao's PNLFM MIMO radar signals which are proposed in (Gao et al. 2017) . All the PNLFM MIMO radar signals proposed in this paper have the same time-frequency scheme as shown in Figure 4(b) without duration gaps. Assuming that $T_\mathrm{p} = 1\mu$s, $B_\mathrm{p} = 400$Mhz, $M = 4$, and $L = 8$. Therefore, $\zeta = 20/T_\mathrm{p} = 2 \times 10^7$, and the total pulse duration of MIMO radar signal is $T = 8\mu$s, there are four transmitting and receiving antennas in our array, respectively. The parameters in the fitness function of genetic algorithm are initialized, the initial population includes 100 individuals, the crossover rate is set to be 0.9, the mutation rate is set to be 0.4, and the iteration number is set to be 200. The weighting coefficients in the fitness function can be set as $\sigma_1 = \sigma_3 = 1$, and $\sigma_2 = 3$, $d_\mathrm{t} = 2\lambda$ and $d_\mathrm{r} = \lambda/2$, The original Gao's PNLFM MIMO radar signals have the time-frequency scheme as shown in Figure 4(a). $T_\mathrm{p} = 0.4\mu$s and $T_\mathrm{r} = 1\mu$s are set in this situation. Therefore, all the different PNLFM MIMO radar signals mentioned above have the same time-bandwidth products.

**Table 2.** Comparison between different PNLFM MIMO radar signals.

Category	$\tau \leq 0.4|T_\mathrm{p}|$		$\tau > 0.4|T_\mathrm{p}|$		ISLS(dB)	ASLS(dB)	AVDC(dB)
	APSLS(dB)	CSLS(dB)	APSLS(dB)	CSLS(dB)			
Original Gao's PNLFM MIMO radar signal	-41.34	-22.08	-21.82	-22.23	-38.86	-13.45	-1.18
Gao's PNLFM MIMO radar signal	-29.40	-24.47	-25.82	-24.38	-38.73	-13.34	-0.46
Gao's PNLFM MIMO radar signal with improvement	-29.50	-25.45	-25.56	-24.93	-38.37	-13.34	-0.46
Zhao's PNLFM MIMO radar signal	-29.98	-25.29	-24.12	-25.11	-38.08	-13.34	-0.40
New PNLFM MIMO radar signal	-29.98	-23.74	-26.08	-23.44	-38.46	-13.34	-0.41
PNLFM MIMO radar signal with distinctive waveforms	-30.66	-27.21	-27.18	-26.50	-38.44	-13.34	-0.38

When all the subcarrier sequence number $Y_{m,l} = 1$, the new signals are composed of Gao's PNLFM waveforms which have been improved, and they can be labelled as Gao's PNLFM MIMO radar signal with improvement. When all the subcarrier sequence number $Y_{m,l} = 2$, the new signals are composed of Zhao's PNLFM waveforms, and they can be labelled as Zhao's PNLFM MIMO radar signal. When all the subcarrier sequence number $Y_{m,l} = 3$, the new signals are composed of our new proposed PNLFM waveforms, and they can be labelled as New PNLFM MIMO radar signal. In addition, according to the optimization of fitness function, the best subcarrier sequence number is obtained as $\mathbf{Y}$={2,3,3,2,2,2,2,1;3,3,3,1,1,2,2,2,1;1,2,3,1,2,2,2,3;3,3,2,3,2,2,1,1;}. Then we can obtain our proposed PNLFM MIMO radar signals, and they can be nominated as PNLFM MIMO radar signal with distinctive waveforms. Here, Gao's PNLFM MIMO radar signals mean that they have the time-frequency scheme as shown in Figure 4(b) and their PNLFM subcarriers are the waveforms proposed in (Gao et al. 2017) without any improvement.

Figure (5) shows the ACF and CCF of different PNLFM MIMO radar signals, and Figure (6) shows the ACF and CCF of different PNLFM MIMO radar signals in their mainlobes. As shown in Equation (25), the range of mainlobe is $\tau \leq 0.2|T_\mathrm{p}|$. When $\tau > 0.4|T_\mathrm{p}|$ and $\tau \leq 0.4|T_\mathrm{p}|$, the APSLs and CSLs are both shown in Table (2). It can be observed that original Gao's PNLFM MIMO radar signals have the highest APSLs and CSLs when $\tau > 0.4|T_\mathrm{p}|$, the high repetitive sidelobes are produced by the duration gaps between each subcarrier and each subcarrier has the same expression. It can be noted that they have the lowest APSLs but highest CSLs in their mainlobes. When
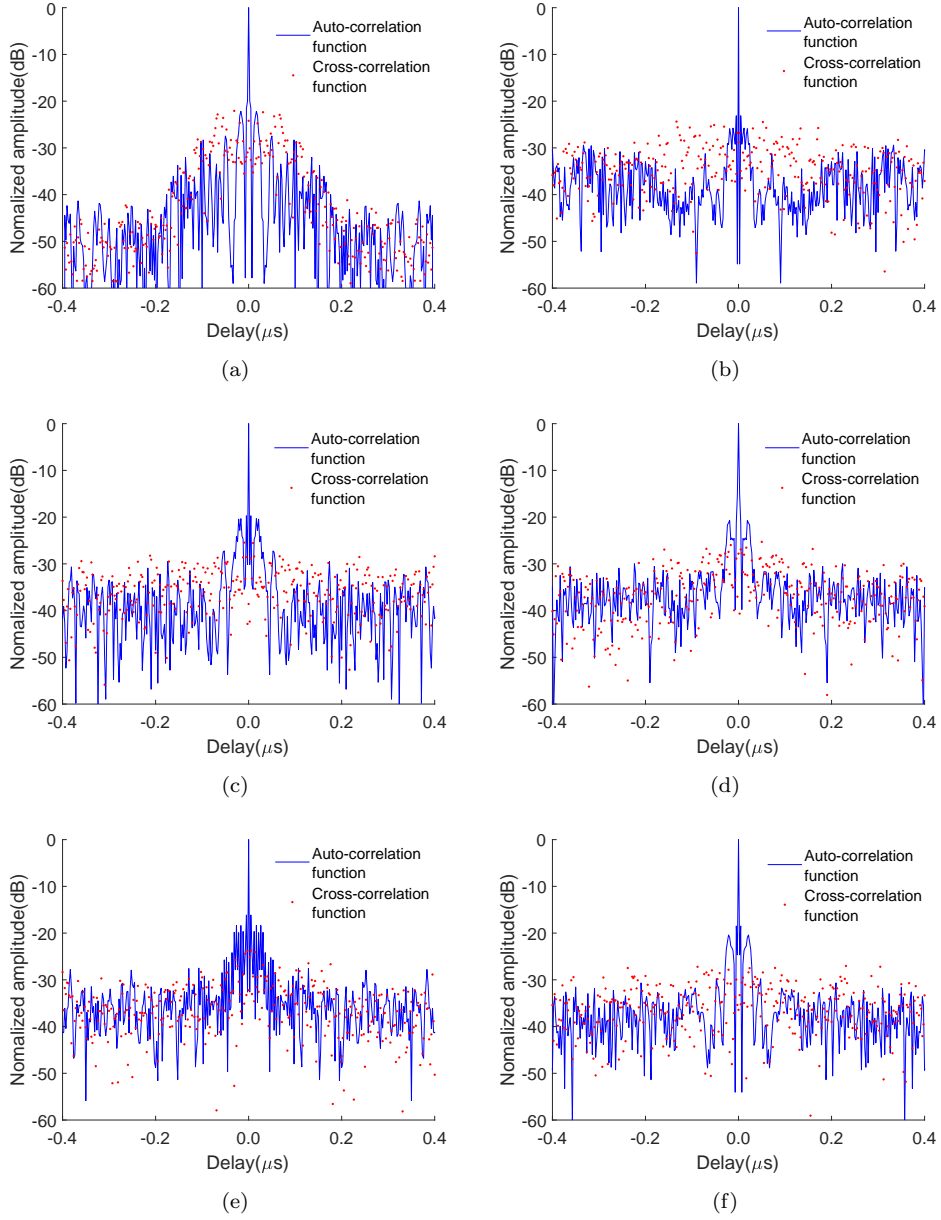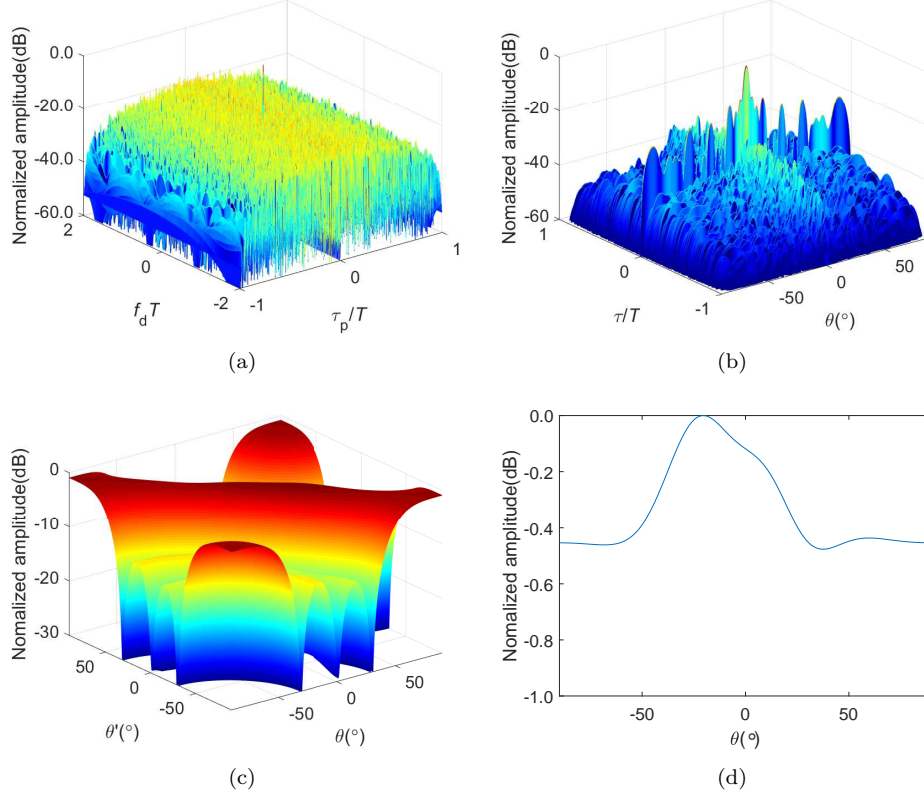
Figure 6. The mainlobe of ACF and CCF of PNLFM MIMO radar signals. (a) Original Gao's PNLFM MIMO radar signal. (b) Gao's PNLFM MIMO radar signal. (c) Gao's PNLFM MIMO radar signal with improvement. (d) Zhao's PNLFM MIMO radar signal. (e) New PNLFM MIMO radar signal. (f) PNLFM MIMO radar signal with distinctive waveforms.

(a)

(b)

(c)

(d)
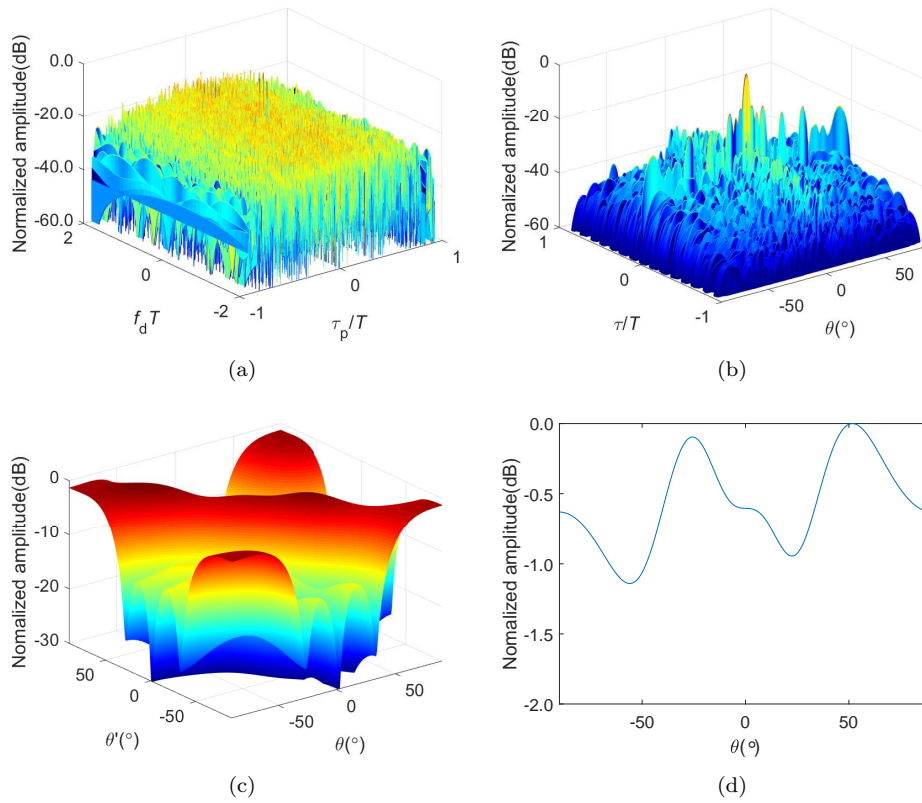
Figure 7. The properties of original Gao's PNLFM MIMO radar signals. (a) The ambiguity function of original Gao's PNLFM MIMO radar signal. (b) The range angle function of original Gao's PNLFM MIMO radar signal. (c) The transmitting beampattern of original Gao's PNLFM MIMO radar signal. (d) The diagonal cut of the transmitting beampattern of original Gao's PNLFM MIMO radar signal.

15

the target locates near the mainlobe with high signal noise ratio(SINR), the target can be detected easily, otherwise it will lose its advantage. When the duration gaps of time-frequency scheme as shown in Figure 4(b) are eliminated, it can be observed that the APSLs become more average during the whole period of the time delay. All the signals in this kind of time-frequency scheme have almost the same APSLs in their mainlobes. According to the method with distinctive subcarriers within the whole signal, our proposed PNLFM MIMO radar signals have the lowest APSLs and CSLs in the whole period of time delay.
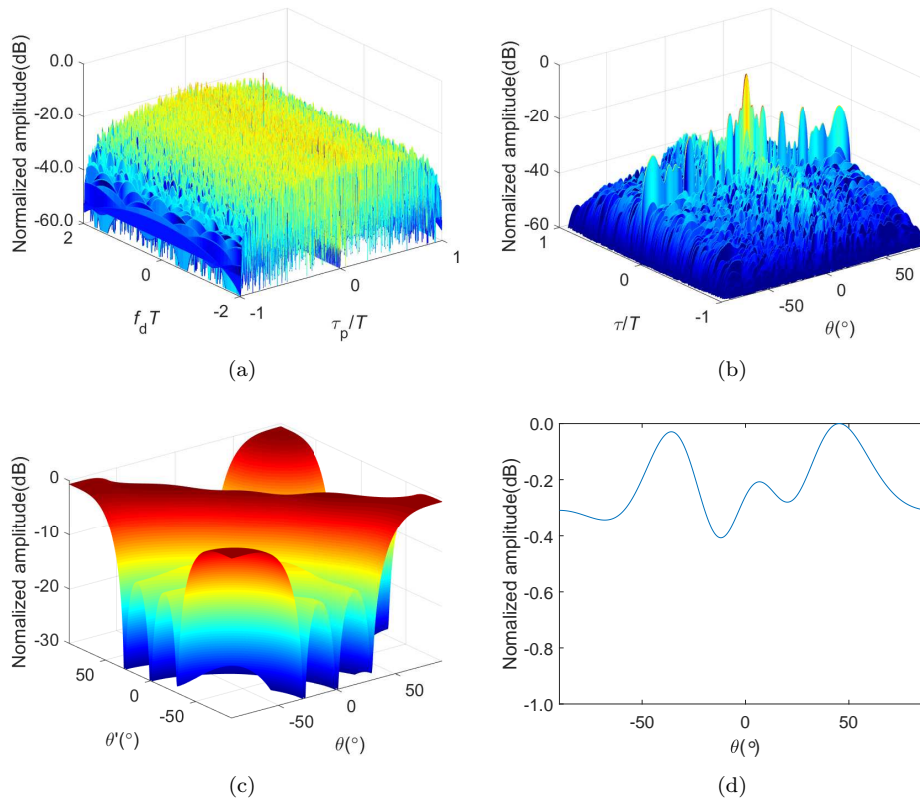

Figure 8. The properties of Gao's PNLFM MIMO radar signals with improvement. (a) The ambiguity function of Gao's PNLFM MIMO radar signal with improvement. (b) The range angle function of Gao's PNLFM MIMO radar signal with improvement. (c) The transmitting beampattern of Gao's PNLFM MIMO radar signal with improvement. (d) The diagonal cut of the transmitting beampattern of Gao's PNLFM MIMO radar signals with improvement.

It can be observed that all the PNLFM MIMO radar signals that consist of only one kind of subcarriers produce high repetitive sidelobes both in ACF and CCF. In our proposed PNLFM MIMO radar signals with distinctive waveforms, there are three different kinds of subcarriers. They are Gao's PNLFM waveforms with improvement, Zhao's PNLFM waveforms, and our novel designed PNLFM waveforms, respectively. Each different waveform has its own controllable parameters, the degrees of freedom are increased significantly in our proposed PNLFM waveforms. In addition, the sequence number of each subcarrier is selected randomly. According to the optimization of genetic algorithm, our proposed PNLFM MIMO radar signals can achieve better performance than the others.

Here, some other properties of the signals are simulated, which include the ambiguity

16

Figure 9. The properties of Zhao's PNLFM MIMO radar signals. (a) The ambiguity function of Zhao's PNLFM MIMO radar signal. (b) The range angle function of Zhao's PNLFM MIMO radar signal. (c) The transmitting beampattern of Zhao's PNLFM MIMO radar signal. (d) The diagonal cut of the transmitting beampattern of Zhao's PNLFM MIMO radar signal.

17
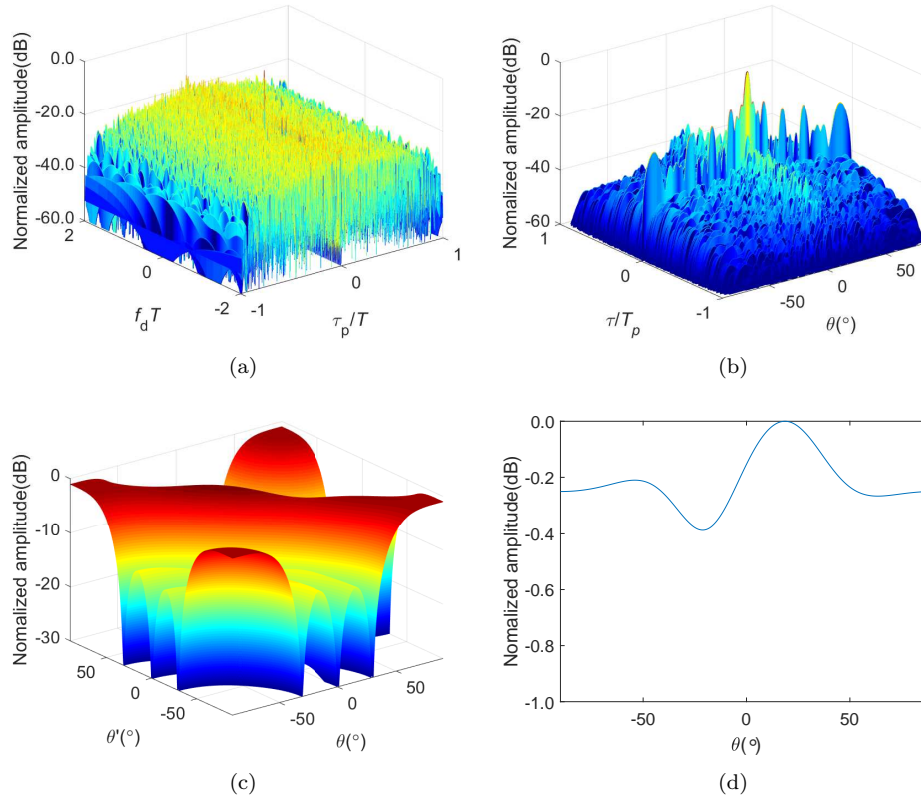
Figure 10. The properties of PNLFM MIMO radar signals with distinctive waveforms. (a) The ambiguity function of PNLFM MIMO radar signal with distinctive waveforms. (b) The range angle function of PNLFM MIMO radar signal with distinctive waveforms. (c) The transmitting beampattern of PNLFM MIMO radar signal with distinctive waveforms. (d) The diagonal cut of the transmitting beampattern of PNLFM MIMO radar signal with distinctive waveforms.

18

function, range angle function, transmitting beampattern and the diagonal cut of its transmitting beampattern. Since some signal have very similar properties, we choose to show the original Gao's PNLFM MIMO radar signals, Gao's PNLFM MIMO radar signals with improvement, Zhao's PNLFM MIMO radar signals and our proposed PNLFM MIMO radar signals with distinctive waveforms. The simulations of each signal are shown in Figure (7), Figure (8), Figure (9) and Figure (10), respectively, and the simulation results are shown in Table (2). It can be observed that there are two high sidelobes in the direction of Doppler delay in Figure 7(a), it means that original Gao's PNLFM MIMO radar signals are very sensitive to the Doppler shift. However, the ambiguity functions of the other signals are like thumb-tack and have good properties in the direction of both range and Doppler delay. From Table (2), we can see that all the signals almost have the same ISLs and ASLs, meaning that they have almost the same detection ability of targets in the aspect of radar transmitting power and different angles. The diagonal cut of the transmitting beampattern of each PNLFM MIMO radar signal shows the orthogonality, and when the amplitude variation of the diagonal cut(AVDC) reduces, the ability of orthogonality improves. According to the results from Table (2), original Gao's PNLFM MIMO radar signals have the biggest variation range, and all the other signals have almost the same variation range. The PNLFM MIMO radar signals with distinctive waveform have the smallest variation range, therefore they have the best orthogonal characteristics. In a summary, according to the simulation results mentioned above, our proposed MIMO radar signals with distinctive waveforms achieve improved performance, in comparison to those analysed here.

6.   Conclusion

In this paper, a new PNLFM MIMO radar signal has been proposed for MIMO radar. The simulation results illustrate that the repetitive high sidelobes caused by the same subcarrier durations have been suppressed by the genetic algorithm with different categories of subcarriers. Our proposed new waveforms have lower APSLS, CSLS and ASLs. They also have the smallest variation range of the diagonal cut of the transmitting beampattern. This means that our proposed PNLFM MIMO radar signals with distinctive waveforms have the improved orthogonality. In addition, there are more degrees of freedom in our proposed signals and improve the diversity of MIMO radar signals significantly. Therefore, our proposed signal can be applied into more powerful MIMO radar against challenging targets.

References

Boukeffa, S., Y. Jiang and T. Jiang. 2011. "Sidelobe reduction with nonlinear frequency modulated waveforms," *2011 IEEE 7th International Colloquium on Signal Processing and its*

Applications, 399-403.

Cao, Y., X. Xia and S. Wang. 2015. "IRCI free colocated mimo radar based on sufficient cyclic prefix OFDM waveforms," *IEEE Transactions on Aerospace and Electronic Systems*, 51 (3) 2107-2120.

Cerutti-Maori, D., I. Sikaneta, J. Klare and C. H. Gierull. 2014. "MIMO SAR Processing for Multichannel High-Resolution Wide-Swath Radars," *IEEE Transactions on Geoscience and Remote Sensing*, 52 (8) 5034-5055.

Chen, C. and P. P. Vaidyanathan. 2008. "MIMO Radar Ambiguity Properties and Optimization Using Frequency-Hopping Waveforms," *IEEE Transactions on Signal Processing*, 56 (12) 5926-5936.

Fan, W., J. Liang and J. Li. 2018. "Constant Modulus MIMO Radar Waveform Design With Minimum Peak Sidelobe Transmit Beampattern," *IEEE Transactions on Signal Processing*, 66 (16) 4207-4222.

Fuhrmann, D. R. and G. S. Antonio. 2008. "Transmit beamforming for MIMO radar systems using signal cross-correlation, *IEEE Transactions on Aerospace and Electronic Systems*, 44 (1) 171-186.

Gao, C., K. C. Teh, A. Liu and H. Sun. 2016. "Piecewise LFM waveform for MIMO radar," *IEEE Transactions on Aerospace and Electronic Systems*, 52 (2) 590-602.

Herbert, S., J. R. Hopgood and B. Mulgrew. 2018. "MMSE Adaptive Waveform Design for Active Sensing With Applications to MIMO Radar," *IEEE Transactions on Signal Processing*, 66 (5) 1361-1373.

Gao, C., K. C. Teh and A. Liu. 2017. "Piecewise Nonlinear Frequency Modulation Waveform for MIMO Radar," *IEEE Journal of Selected Topics in Signal Processing*, 11 (2) 379-390.

Hu, X., N. Tong, Y. Zhang and D. Huang. 2018. "MIMO Radar Imaging With Nonorthogonal Waveforms Based on Joint-Block Sparse Recovery," *IEEE Transactions on Geoscience and Remote Sensing*, 56 (10) 5985-5996.

Hua, G. and S. S. Abeysekera. 2013. "MIMO radar transmit beampattern design with ripple and transition band control, *IEEE Transactions on Signal Processing*, 61 (11) 2963-2974.

Kim, J., M. Younis, A. Moreira and W. Wiesbeck. 2015. "Spaceborne MIMO Synthetic Aperture Radar for Multimodal Operation," *IEEE Transactions on Geoscience and Remote Sensing*, 53 (5) 2453-2466.

Krieger, G. 2014. "MIMO-SAR: Opportunities and Pitfalls," *IEEE Transactions on Geoscience and Remote Sensing*, 52 (5) 2628-2645.

Liu, B., Z. He and Q. He. 2007. "Optimization of Orthogonal Discrete Frequency-Coding Waveform Based on Modified Genetic Algorithm for MIMO Radar," *2007 International Conference on Communications, Circuits and Systems*, 966-970.

Moo, P. W. and Z. Ding. 2013. "Tracking Performance of MIMO Radar for Accelerating Targets," IEEE Transactions on Signal Processing, 61 (21) 5205-5216.

Song, X., S. Zhou and P. Willett. 2010. "Reducing the Waveform Cross Correlation of MIMO Radar With SpaceTime Coding," *IEEE Transactions on Signal Processing*, 58 (8) 4213-4224.

Stoica, P., J. Li, and X. Zhu. 2008. "Waveform synthesis for diversity-based transmit beampattern design, *IEEE Transaction on Signal Processing*, 56 (6) 2593-2598.

Tarchi, D., F. Oliveri and P. F. Sammartino. 2013. "MIMO Radar and Ground-Based SAR Imaging Systems: Equivalent Approaches for Remote Sensing," *IEEE Transactions on Geoscience and Remote Sensing* 51 (1) 425-435.

Wang, J., L. Chen, X. Liang, C. Ding and K. Li, "Implementation of the OFDM Chirp Waveform on MIMO SAR Systems," IEEE Transactions on Geoscience and Remote Sensing, vol. 53, no. 9, pp. 5218-5228, Sept. 2015.

Wang, W.. 2015. "MIMO SAR OFDM Chirp Waveform Diversity Design With Random Matrix Modulation," *IEEE Transactions on Geoscience and Remote Sensing*, 53 (3) 1615-1625.

Yang, Y. and R. S. Blum. 2007. "MIMO radar waveform design based on mutual information and minimum mean-square error estimation," *IEEE Transactions on Aerospace and Electronic Systems*, 43 (1) 330-343.

Yang, Y. and R. S. Blum. 2007. "Minimax Robust MIMO Radar Waveform Design," *IEEE*

Journal of Selected Topics in Signal Processing, 1 (1) 147-155.

Zhao, Y., X. Lu, J. Yang, W. Su and H. Gu. 2018. "OFDM waveforms designed with piecewise nonlinear frequency modulation pulse for MIMO radar" *International Journal of Remote Sensing*, 39 (23) 8746-8765.